APPLIED SCIENCES AND ENGINEERING

Spatiotemporal single-cell tracking analysis in 3D tissues to reveal heterogeneous cellular response to mechanical stimuli

Keitaro Kasahara[1]†, Jumpei Muramatsu[1], Yuta Kurashina[2,3], Shigenori Miura[4]‡, Shogo Miyata[2], Hiroaki Onoe[2]*

Mechanical stimuli have been recognized as important for tissue maturation, homeostasis and constructing engineered three-dimensional (3D) tissues. However, we know little about the cellular mechanical response in tissues that could be considerably heterogeneous and spatiotemporally dynamic due to the complex structure of tissues. Here, we report a spatiotemporal single-cell tracking analysis of in vitro 3D tissues under mechanical stretch, to reveal the heterogeneous cellular behavior by using a developed stretch and optical live imaging system. The system could affect the cellular orientation and directly measure the distance of cells in in vitro 3D myoblast tissues (3DMTs) at the single-cell level. Moreover, we observed the spatiotemporal heterogeneous cellular locomotion and shape changes under mechanical stretch in 3DMTs. This single-cell tracking analysis can become a principal method to investigate the heterogeneous cellular response in tissues and provide insights that conventional analyses have not yet offered.

INTRODUCTION

Muscles and bones composing our body are constantly exposed to mechanical stimuli such as gravity, physical activity, and exercise, which are indispensable for maintaining enough body strength (*1*, *2*). Likewise, most cells and tissues building our body are subjected to mechanical stimuli, for example, stretching and shear stress (*3*, *4*). These mechanical stimuli are sensed by receptors on the cellular membrane and converted into biochemical signals, altering various cellular behaviors including proliferation, differentiation, and apoptosis (*5*–*7*). This mechanical response of cells and tissues has recently been applied to constructing engineered three-dimensional (3D) tissues that are promising to mimic the function and structure of in vivo tissues (*8*, *9*). Tissue-scale responses to mechanical stimuli, notably alignment, differentiation, and maturation, have already been reproduced with in vitro 3D tissue models (*10*–*13*).

Mechanical response of in vitro 3D tissues is often evaluated by observation of tissue structure, e.g., immunostaining, or by quantitative analysis, e.g., Western blot (*14*–*16*). Most of these methods focus on the mechanical response at the tissue scale; in other words, they evaluate the mechanical response by averaging the behavior of each cell that composes a tissue. In reality, however, the behavior of cells in a 3D tissue could be considerably heterogeneous and spatiotemporally dynamic because each cell is assumed to adhere to the surrounding extracellular matrix (ECM) and other cells differently at different time points. The actual mechanical stimuli applied to each cell could be in various directions with different intensities as a result of heterogeneous cellular adhesion and tissue formation. Recently, the heterogeneous cellular behavior of single cells in a complex multicellular system has been reported to influence collective cell behavior at the multicellular level. For instance, it was reported that heterogeneity of local elasticity, cell density, and cell-cell interactions affects the mechanical stress field distribution, collective cell migration, traction stresses, proliferation, and apoptosis (*17*–*19*). The importance of heterogeneous cellular activity has also been recognized in various cancer and tumor research using single-cell analysis in microenvironments (*20*, *21*). Focusing on the heterogeneous cellular behavior allows us to investigate how each unique cell responds to mechanical stimuli that are applied to a tissue, leading to a comprehensive understanding of the cell-tissue concerted multiscale response. To investigate cellular response in an in vitro 3D tissue to mechanical stimuli with a focus on cellular behavioral heterogeneity, an experimental system is required such that it enables us to track specific single cells in an in vitro 3D tissue at a single-cell scale while culturing the 3D tissue under mechanical stimuli simultaneously.

Here, we conduct a spatiotemporal single-cell tracking analysis of in vitro 3D tissues subjected to mechanical stretch to reveal the heterogeneous cellular behavior by using a developed optical live imaging and stretch system. In the process of tissue-level mechanical response such as cellular alignment, we hypothesize that there are several steps connecting multiscale reactions beginning from cells and propagating to tissues (Fig. 1). First, (i) mechanical stimuli are applied on each cell as different inputs due to the heterogeneous structure of 3D tissue, and, then, (ii) cells react to mechanical stimuli heterogeneously depending on each mechanical input [for example, cells staying in the same shape, rotating cells, and

[1]School of Integrated Design Engineering, Graduate School of Science and Technology, Keio University, 3-14-1 Hiyoshi, Kohoku-ku, Yokohama 223-8522, Japan. [2]Department of Mechanical Engineering, Faculty of Science and Technology, Keio University, 3-14-1 Hiyoshi, Kohoku-ku, Yokohama 223-8522, Japan. [3]Division of Advanced Mechanical Systems Engineering, Institute of Engineering, Tokyo University of Agriculture and Technology, 2-24-16 Nakacho, Koganei-shi, Tokyo 184-8588, Japan. [4]Department of Mechano-Informatics, Graduate School of Information Science and Technology, The University of Tokyo, 7-3-1 Hongo, Bunkyo-ku, Tokyo 113-8656, Japan.
*Corresponding author. Email: onoe@mech.keio.ac.jp
†Present address: Institute of Bio- and Geosciences, IBG-1: Biotechnology, Forschungszentrum Jülich GmbH, Jülich, Germany; Wilhelm-Johnen-Straße, 52425 Jülich, Germany.
‡Present address: Department of Molecular Biology and Biochemistry, Graduate School of Biomedical and Health Sciences, Hiroshima University, Hiroshima 734-8553, Japan.

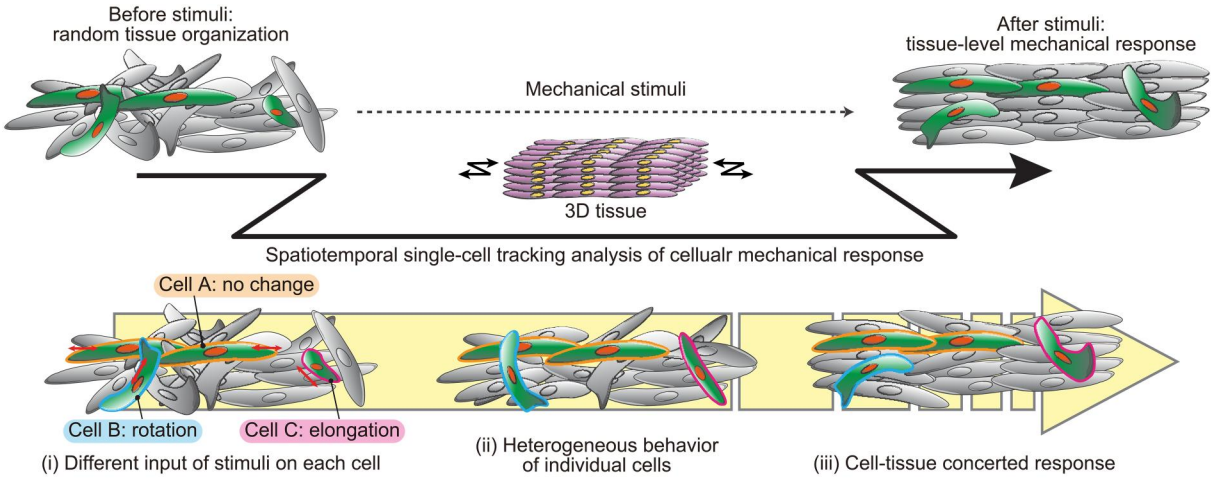

Fig. 1. Conceptual illustration of single-cell live analysis of spatiotemporal mechanical response. During the mechanical stimuli, each cell composing a 3D tissue is assumed to experience various inputs of stimuli due to the heterogeneous tissue structure, leading to heterogeneous cellular behavior before the mechanical response is visible at the tissue level.

elongating cells (Fig. 1)], which lastly lead to (iii) cell-tissue concerted response. Through the single-cell tracking analysis, we demonstrate that cellular heterogeneity exists in mechanically stimulated 3D tissues and nonstimulated 3D tissues. A certain number of fluorescently labeled cells in a 3D tissue were observed with confocal microscopy while being subjected to mechanical stretch, enabling single-cell–level tracking analysis of cellular behavior. Briefly, the developed system is composed of a 3D tissue that is constructed inside a polydimethylsiloxane (PDMS) stretch chamber and two linear motorized stages to apply uniaxial stretch on the 3D tissue from both sides. The system can be mounted on confocal microscopy so that the target cells in the 3D tissue can be continuously observed at high resolution during culture with mechanical stretch. We used the mouse C2C12 myoblast cells to validate the performance of the presented device. First, we examined cellular orientation in the 3D myoblast tissues (3DMTs) to prove that whole-tissue behavior could be influenced by the stretch with the linear motorized stages. Then, the stretch and live imaging system was verified by measuring the actual stretching ratio of the 3DMTs at a single-cell scale. After the verification of the system, specific cells in 3DMTs were continuously tracked at single-cell resolution while culturing the tissue under stretch simultaneously to reveal heterogeneous cellular response to mechanical stretch.

RESULTS

3D tissue culture in PDMS stretch chamber

To construct stretchable 3DMTs, we used a PDMS stretch chamber fabricated by PDMS molding and two-layer bonding (Fig. 2A and fig. S1). The chamber is composed of two layers: a top layer serving as a medium reservoir and a bottom membrane layer for 3D tissue construction (Fig. 2A and fig. S1). The bottom layer has a 200-μm-deep square hollow for 3D tissue structuring and 600-μm-height pillars to hold a 3D tissue and avoid tissue shrinkage during cell culture and stretch. For 3D tissue construction, ECMs serving as a scaffold for cellular growth are inevitable (*22*, *23*). The mixture of collagen and Matrigel was used in a ratio of 9:1 as an ECM because the mixed ECM of collagen and Matrigel promoted the growth and differentiation of C2C12 (*24*). Cell suspension with ECM was filled in the hollow on the bottom layer and then incubated with the medium in the medium reservoir. The C2C12 cells (Fig. 2B) were cultured in ECM (day 0), and 3D tissue was structured after culturing for 2 days (day 2). It is implied that cells adhered to surrounding cells and ECM during cell culture, forming a square-shaped 3D tissue around the pillars. The zoomed image (Fig. 2C) also shows that cells elongated in various directions to form 3DMTs. For optical live imaging experiments, we introduced plasmid DNA into C2C12 cells by transfection, labeling cell membrane with enhanced green fluorescent protein (EGFP) and nuclei with mCherry. As the efficiency of transfection was around 10 to 15% (fig. S2), it is possible to prepare a mixture of cells with labeled cells and nonlabeled cells. By using this cell mixture for 3D tissue construction, labeled cells in the 3D tissue can be exclusively observed with fluorescence microscopy while being surrounded by nonlabeled cells. We used this feature as a tool to label a certain amount of cells and to enable single-cell imaging for 3D tissues. Therefore, the zoomed image of 3D tissue (Fig. 2C) can be observed fluorescently (Fig. 2D), where only a certain amount of cells composing the 3D tissue was exclusively observed with fluorescence microscopy. The confocal fluorescence image validated the fluorescence localization on the membrane (fig. S2C).

Design of optical live imaging system with stretch

To conduct stretch culture with the fabricated PDMS stretch chamber and 3DMTs, we used a stretch machine composed of two linear motorized stages for a uniaxial stretch that has been developed in previous research (*25*). The stretch machine can be used for stretch culture in an incubator or can be installed into the optical live imaging system with confocal microscopy (Fig. 3, A and B). Cyclic stretch can be applied from both sides of the 3D tissue, enabling the observation of the targeted cell for live tracking analysis in the 3D tissue during the stretch. To estimate the stress distribution in 3DMTs, the mechanical stress induced by 10% stretch was numerically calculated using the experimentally derived Young's modulus of ECM (E = 729 Pa; fig. S3, A to E, and Supplementary

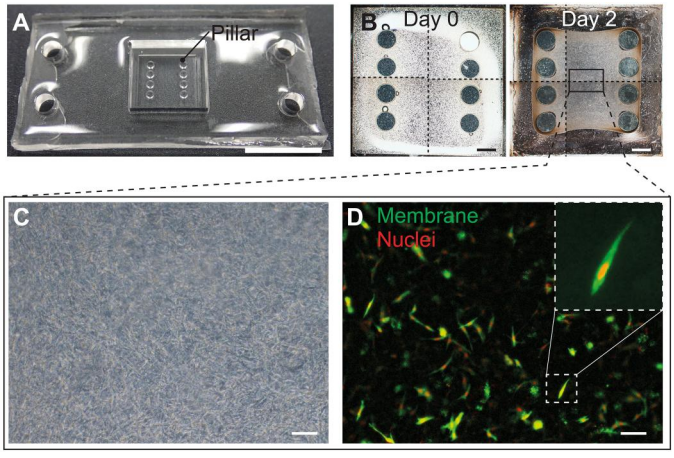

Fig. 2. PDMS stretch chamber fabrication and cell culture. (**A**) Image of the fabricated PDMS stretch chamber (scale bar, 10 mm). (**B**) Cell culture in the PDMS stretch chamber on days 0 and 2. The dashed lines indicate the boundaries of four images manually assembled to obtain the large images (scale bars, 1 mm). (**C**) Cultured cells in the 3D tissue observed by phase contrast microscopy (scale bar, 100 μm). (**D**) Fluorescence microscopic image of cells. Cell membrane and nuclei were labeled with enhanced green fluorescent protein (EGFP) and mCherry, respectively (scale bar, 100 μm).

Materials and Methods). The calculation result showed that homogeneous mechanical stress could be applied at the central area (2 mm by 2 mm) of 3DMTs (average stress of 131 ± 7 Pa, maximum stress of 157 Pa, and minimum stress of 115 Pa; fig. S3F). Together with confocal microscopy and exclusively labeled C2C12 cells, the system allows us to track the spatiotemporal mechanical response of targeted cells in 3DMTs.

Multicell-scale cellular response to stretch

In 3D tissues under mechanical stretch, cells have been known to align in the direction of stretch (*26*–*28*). To check whether our stretch machine could influence cellular behaviors in 3D tissues, 3DMTs were cultured under cyclic stretch (10% of the stretch chamber, 1 Hz) for 12 hours in an incubator, and cellular orientation to the stretch direction was evaluated. The *z*-stack images were acquired with confocal microscopy right before (t = 0 hours) and after (t = 12 hours) the stretch culture with confocal microscopy. The acquired *z*-stack was projected into one image, and, then, the direction of the nuclei was evaluated by image analysis. We also cultured 3DMTs without stretch for comparison. The representative images of 3DMTs cultured under 12 hours of stretch and without stretch were shown, respectively (Fig. 4, A and B). From these images, the angle of nuclei from the stretch direction (angle of 0°) was measured and summarized into histograms (Fig. 4, C and D). The histograms indicate that the evenly distributed angle at t = 0 hours shifted toward the stretch direction after the 12-hours stretch culture (Fig. 4C). In cultures without stretch, on the other hand, no shift was observed in the nuclei angle (Fig. 4D). Moreover, the Kolmogorov-Smirnov (K-S) test showed the significant difference ($P < 0.01$) on the histograms in Fig. 4C (with stretch) at t = 0 hours and t = 12 hours, whereas the K-S test showed no significance on the histograms in Fig. 4D (without stretch) at t = 0 hours and t = 12 hours. These results validate that the stretch machine could influence cellular behaviors in 3DMTs by altering the angle of nuclei

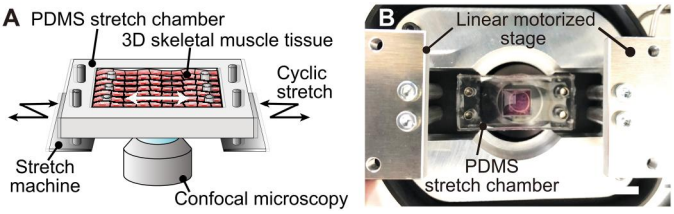

Fig. 3. Optical live imaging system with mechanical stretch. (**A**) The conceptual illustration of the system. (**B**) Image of the constructed system on confocal microscopy (scale bar, 10 mm).

parallel to the stretch direction at a multicell scale. It was also analyzed whether cellular behavior differed depending on the *z* position of the 3DMTs, showing similar tendencies in any *z* positions (fig. S4).

Single-cell–scale analysis: Cell displacement and elongation in 3DMTs under static stretch

Next, the stretch machine was integrated into the optical live imaging system with confocal microscopy to conduct single-cell observation of cellular mechanical response. The representative confocal images of cells in 3DMTs under different applied strains ($S_{machine}$ = 0, 5, and 10%) are shown (Fig. 5A). Here, collagen in the ECM was stained with blue fluorescence to examine whether the ECM structure surrounding cells were heterogeneously structured. The angle of collagen fibers to the direction of stretch (0°) was visualized (Fig. 5B), and the distribution was summarized (Fig. 5C). The result shows that more collagen fibers oriented toward the direction of stretch when subjected to higher $S_{machine}$. Next, intensity profiles were measured from three different positions (positions 1, 2, and 3) in the image of the collagen fiber subjected to $S_{machine}$ = 10% (Fig. 5D). The result showed that the intensity profile differed depending on the positions, implying the heterogeneous distribution of collagen fibers in 3D tissues. Therefore, we assume that cells attach to the heterogeneously structured ECM, leading to heterogeneous attachment and mechanical input.

To evaluate the relationship between the applied stretch ratio ($S_{machine}$) and the measured stretch ratio on 3D tissue (S_{tissue}), we measured the distance of two cells observed through live imaging under static stretch. Static stretch means that the 3D tissue was stretched once (5 or 10%) and maintained the elongated state. The initial distance in stretch direction, d_0, and the distances under stretch (5 and 10%), d, were measured from acquired images to calculate $S_{tissue} = (d - d_0)/d_0$. Note that only cell pairs with $d_0 > 50$ μm were selected and analyzed to avoid direct cellular interaction between cell pairs (Fig. 5E). The calculated S_{tissue} was plotted over $S_{machine}$ as a boxplot (Fig. 5F). The dashed line shows that the ratio is equal to the applied stretch ($S_{tissue} = S_{machine}$). From the boxplot, it was shown that S_{tissue} increased as $S_{machine}$ increased. The mean values were S_{tissue} = 2.4% when $S_{machine}$ = 5% and S_{tissue} = 6.9% when $S_{machine}$ = 10%. This result implies that 3DMTs were stretched in the ratio below the applied stretch as a general trend. Contrary to the general trend, there were also some cell pairs revealing outstanding S_{tissue}, such as S_{tissue} larger than $S_{machine}$ (S_{tissue} = 7.2 and 7.4% when $S_{machine}$ = 5%, and S_{tissue} = 14.5 and 14.7% when $S_{machine}$ = 10%). Even a negative ratio occurred in some cases (S_{tissue} = −4.0 and −3.4% when $S_{machine}$ = 5%). These unexpected results could be caused by the heterogeneous structure in 3D

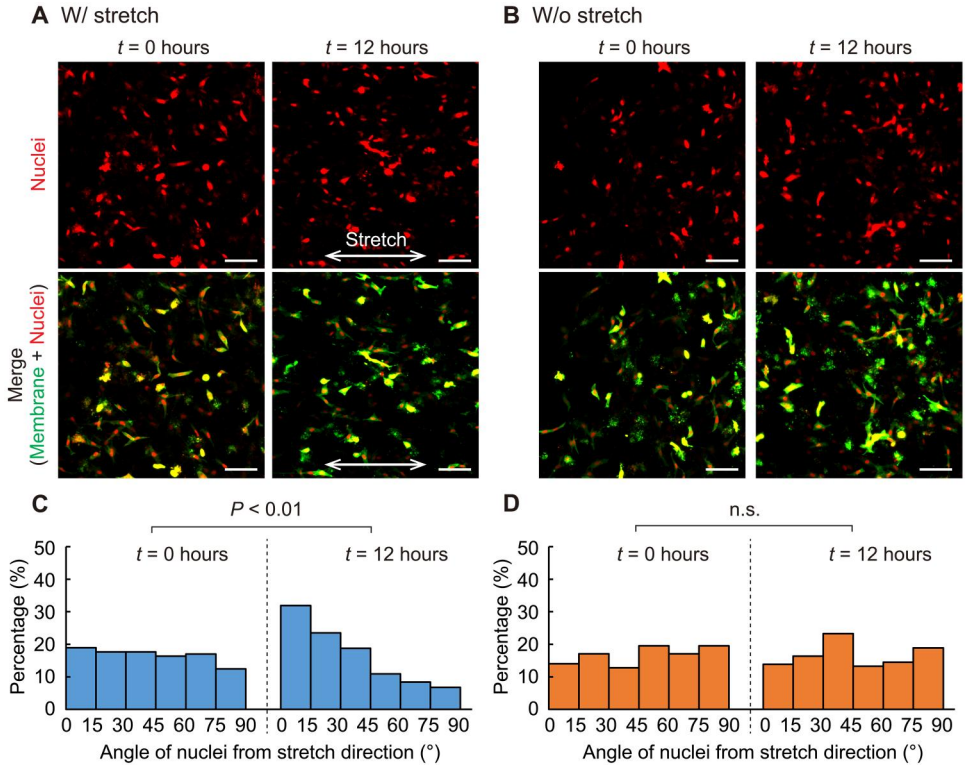

Fig. 4. Multicell-scale analysis: The effect of mechanical stretch on cellular alignment in 3DMTs. (**A**) The fluorescence image of cells in 3DMTs before stretch (t = 0 hours) and after stretch for 12 hours (t = 12 hours). Transfected cells exhibit mCherry on the nuclei (red) and EGFP on the membrane (green). The *z-stack* of images was projected to acquire a single image. The arrow indicates the stretch direction (scale bars, 100 μm). (**B**) The fluorescence image of cells in 3DMTs before (t = 0 hours) and after 12 hours of culture (t = 12 hours) without stretch (scale bars, 100 μm). (**C**) The distribution of the angle from the stretch direction before (t = 0 hours) and after the stretch (t = 12 hours). Data are expressed as means ± SD (t = 0 hours, n = 153 cells; t = 12 hours, n = 358 cells). The Kolmogorov-Smirnov (K-S) test revealed a significant difference in distributions before and after the stretch (P < 0.01). (**D**) The distribution of the angle from the stretch direction before (t = 0 hours) and after 12 hours of culture (t = 12 hours) without stretch. Data are expressed as means ± SD (t = 0 hours, n = 164 cells; t = 12 hours, n = 159 cells).

tissues where cells were assumed to attach to surrounding ECMs and cells irregularly, leading to heterogeneous propagation of the applied stretch over the tissue.

Not only cell displacement but also cell elongation could be analyzed with the proposed optical live imaging system. The acquired fluorescence images of the cell membrane (green) under $S_{machine}$ = 0, 5, and 10% were binarized to be used for the analysis of cell elongation (Fig. 5G). The binarized cell was then fitted to an ellipse. The major and minor axis lengths of the fitted ellipse were measured to evaluate cell elongation (S_{cell}) under $S_{machine}$ = 0, 5, and 10%. The lengths of the major axis (a_0, initial length without stretch; a, length with stretch) and the minor axis (b_0, initial length without stretch; b, length w/stretch) were measured to calculate $S_{cell} = (a - a_0)/a_0$ for the major axis and $S_{cell} = (b - b_0)/b_0$ for the minor axis. The evaluated cells could be categorized into two groups by the initial angle of the cell (θ), $0° \leq \theta < 45°$ and $45° < \theta \leq 90°$ (Fig. 5H). Blue circles and orange triangles indicate individual data points ($0° \leq \theta < 45°$, n = 3 cells; $45° < \theta \leq 90°$, n = 4 cells). The blue lines and orange dashed lines indicate the average values. First, cells categorized to $0° \leq \theta < 45°$ were summarized in the top plot. These cells tended to be elongated in the direction of the major axis and compressed in the direction of the minor axis. Then, cells categorized to $45° < \theta \leq 90°$ were summarized in the bottom plot. These cells tended to be elongated in the direction of the minor axis and compressed in the direction of the major axis. The results imply that the direction of elongation is influenced by the initial angle of the cell. Similarly to the analysis of cell displacement, some cells exhibited extraordinary S_{cell}, regardless of the global tendency. One of the cells showed elongation in both the major and minor axes (S_{cell} = 1.9% in the major axis and 5.6% in the minor axis when $S_{machine}$ = 5%, and S_{cell} = 9.6% in the major axis and 14.1% in the minor axis when $S_{machine}$ = 10%).

These findings on cell displacement and elongation led us to the next experiment with the developed optical live imaging and stretch system to evaluate the cellular heterogeneity in 3D tissues under mechanical stretch in detail.

Single-cell tracking analysis in 3D tissues under mechanical stretch

To evaluate whether cells composing a 3D tissue reveal heterogeneous cellular responses to the mechanical stretch, spatiotemporal cellular behavior was tracked at the single-cell level under mechanical stretch using our optical live imaging and stretch system. The PDMS stretch chamber with 3DMT was placed in the system and exposed to uniaxial cyclic stretch (10%, 1 Hz) for 1 hour. After the stretch, cells exhibiting fluorescence signals were observed with confocal microscopy to acquire *z*-stack images. Then, 3DMTs were exposed to the stretch again for 1 hour, followed by confocal observation of the same targeted cells. As we focused

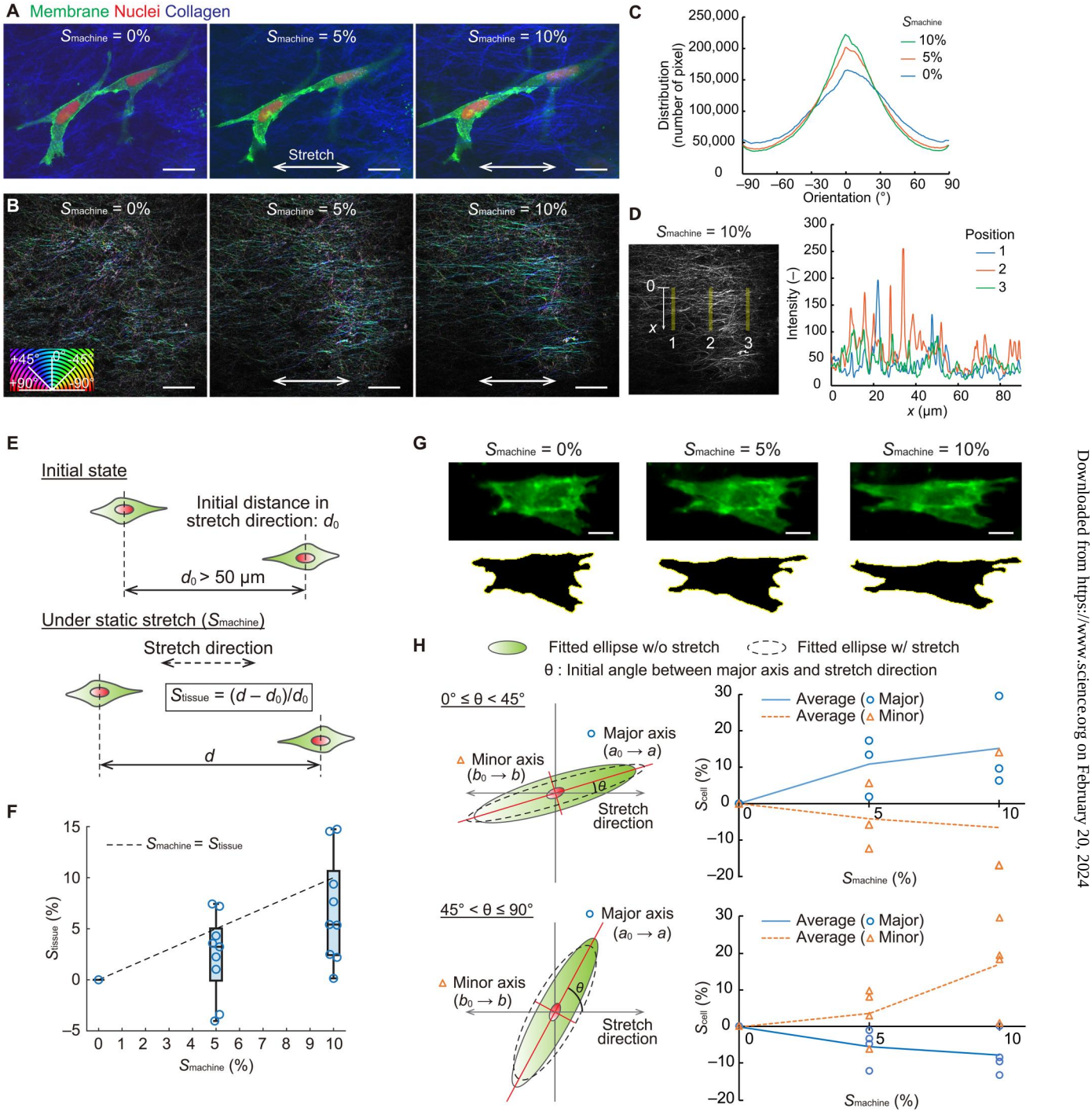

Fig. 5. Single-cell–scale analysis: Displacement and elongation of cells in 3DMTs under static stretch. (**A**) The representative fluorescence images of cells in 3DMTs under different applied strains ($S_{machine}$ = 0, 5, and 10%). Transfected cells exhibit mCherry on nuclei (red) and EGFP on the membrane (green). Collagen in ECM was stained with blue fluorescence (scale bars, 20 μm). (**B**) The orientation analysis of collagen fibers in 3DMTs under $S_{machine}$ = 0, 5, and 10%. The angles of collagen fibers were visualized by color (scale bars, 50 μm). (**C**) The orientation distribution of collagen fibers under $S_{machine}$ = 0, 5, and 10%. (**D**) The intensity profile of three different positions on the fluorescence image of collagen under $S_{machine}$ = 10%). (**E**) The actual stretch ratio was calculated by measuring the distance between two cells with an initial distance larger than 50 μm, without and with stretch. (**F**) The measured stretch ratio (S_{tissue}) to the applied stretch ratio ($S_{machine}$). Boxes have the meaning of 25 and 75% quartile around the population mean value (middle line, median), error bars indicate maximum and minimum, and blue circles indicate individual data points (n = 9). (**G**) The representative fluorescence images of the cell membrane (green) under $S_{machine}$ = 0, 5, and 10%. These images were binarized for the analysis of cell elongation (scale bars, 10 μm). (**H**) The binarized cell was fitted to an ellipse. The major and minor axis lengths were used to evaluate cell elongation under $S_{machine}$ = 0, 5, and 10%. The evaluated cells were categorized into two groups by the initial angle of the cell (θ). Blue circles and orange triangles indicate individual data points (0° ≤ θ < 45°, n = 3 cells; 45° < θ ≤ 90°, n = 4 cells). The blue lines and orange dashed lines indicate the average values.

especially on the initial (6- to 12-hour) cellular adaptation to mechanical stimuli, cells were exposed to cyclic stretch for 6 to 12 hours in total. Previous research on stretch-induced cellular reorientation suggests that the stretch duration of 6 hours is already sufficient to observe and evaluate initial cellular adaptation (*29*–*31*). To visualize the cellular shape for each observation point, the 3D cellular model was reconstructed from the acquired *z*-stack images. Note that the single-cell tracking analysis here was meant to examine whether there is heterogeneity in terms of cellular adaptation to mechanical stimuli.

As control samples, we first cultured 3DMTs in the system without stretch and observed the behavior of targeted cells. The observed cells, cells C_1 and C_2, showed very distinctive behavior. Cell C_1, first of all, was observed with only minor changes in cellular shape (Fig. 6A). The length of the cellular protrusion structure changed, but the overall shape remained the same as the cellular shape at t = 0 hours. Cell C_2, on the other hand, showed a notable movement and ended with a considerably different cellular shape after observation for more than 10 hours (Fig. 6B). To quantitatively analyze the distinctive behavior of cell C_1 and cell C_2, the angle of nuclei was measured for each cell and summarized in a graph (Fig. 6C). The graph indicates that the two cells behaved uniquely; cell C_1 showed small fluctuation in angle, whereas cell C_2 presented marked change, starting from 148° and ending with 20° (Fig. 6C). The observation of cells C_1 and C_2 and five other cells ensured that cellular behavior in an identical 3D tissue is diverse and that the developed system enables us to analyze the heterogeneous cellular behavior by 3D visualization and quantitative measurement.

Then, we observed the other three cells—cells S_1, S_2, and S_3—while culturing 3DMTs under cyclic stretch. First, we focused on differentiated multinucleated cells, S_1 and S_2, growing in the direction of the stretch (Fig. 6D). The cells S_1 and S_2 remained in the direction of the stretch after observation for more than 12 hours, representing the tissue-scale behavior as we observed in the multicell-scale response to stretch (Fig. 4C). Contrary to the behavior of cell S_1 and S_2, we also observed a cell, S_3, exhibiting continuously changing protrusion structure (Fig. 6E). To analyze the different behavior of cells S_1, S_2, and S_3, nuclei angle was measured for each cell and summarized in a graph (Fig. 6F). Note that the stretch direction is equal to angle = 0°, 180°, and 360° (Fig. 6F). The graph indicates that cells S_1, S_2, and S_3 exhibited a different change in nuclei angle; cells S_1 and S_2 remained their nuclei angle close to the stretch direction during the experiment, whereas cell S_3 showed a dynamic change in nuclei angle, starting from 97° and ending with 241° (Fig. 6F). The result obtained from cells S_1, S_2, and S_3 and six other cells implies that cellular heterogeneity exists in 3D tissues subjected to mechanical stretch. The cellular heterogeneity was often neglected through standard evaluation methods such as immunostaining and Western blot. The presented system allows us to investigate how each unique cell responds to mechanical stimuli that are applied to a tissue, leading to a comprehensive understanding of the cell-tissue concerted multiscale response that has been difficult to analyze with previous methods.

Analysis of Golgi marker by spatiotemporal single-cell tracking

To demonstrate our system for more in-depth biological analysis, a spatiotemporal single-cell tracking analysis was performed with a Golgi marker. Golgi is known for its localization toward the direction of cellular migration (*32*, *33*). As our research focuses on initial cellular adaptation to mechanical stimuli, for example, migration in 3D tissues under stretch, the Golgi body marker is a suitable candidate for continuous observation and further in-depth biological analysis.

We observed a cell with Golgi localizing to one side of the nucleus (Fig. 7, A to C). We also observed a cell with Golgi splitting around the nucleus (Fig. 7, D to F). From these two cells, heterogeneity in intracellular organelle localization was observed. As an example of the analysis with the Golgi position, two cells (cells A and B) were selected (Fig. 7G). While cell A was labeled only on the nucleus and membrane, cell B was labeled also on the Golgi. Using these two cells, the relative position of cell B (nucleus and Golgi) from cell A (nucleus) was measured and summarized in a plot (Fig. 7H). The plot clearly shows the spatiotemporal movement of cell B relative to the position of cell A in the 3D space. Then, we looked at the relative position movement in the *xy* plane (Fig. 7I). The movement of cell B in the *x*-axis direction seemed to be directed to the Golgi localization direction. The adverse movement was observed in the *y*-axis direction. The relative position movement in the *xz* plane was also extracted (Fig. 7J). Here, we can see that cell B moved upward until the next observation point (t = 3.6 hours) and then downward in the opposite direction (t = 6.9 hours). The directional change of cell B before and after t = 3.6 hours might have arisen from the strong localization of Golgi toward the $-z$ direction, as indicated by the long dashed arrow. Such real-time 3D movement data could be used for more in-depth biological insight into spatiotemporal organelle localization and accompanying cellular behavior in a mechanically stimulated 3D multicellular environment. Together, it was demonstrated that our system can provide real-time information on single-cell–level organelle localization and cellular migration in a 3D tissue under mechanical stimuli.

DISCUSSION

We successfully observed the heterogeneous cellular behavior under mechanical stretch in in vitro 3DMTs. What has been presented here is distinctive from others in that we aimed to focus on the spatiotemporal behaviors of individual cells composing a 3D tissue rather than evaluating the tissue after finishing the mechanical stimuli. The actual cellular behavior in 3D tissues has often been neglected due to the difficulty to observe and track a single target cell in 3D tissues. The alternative evaluation methods are mostly based on cellular fixation that hinders continuous observation and evaluation of an identical sample (*14*–*16*). Immunostaining and Western blotting, for instance, give us insights into the tissue state before and after the application of the mechanical stimuli, yet they provide little information about cellular heterogeneity. The proposed investigation on cellular heterogeneity by spatiotemporal single-cell tracking analysis is, therefore, unique from other research and gives insights toward further development in the field of tissue engineering, as well as fundamental biology such as developmental biology.

The presented optical live imaging and stretch system enabled us to investigate the cellular mechanical response inside in vitro 3D tissues at a single-cell scale, offering insights into cellular heterogeneity in 3D tissues. Conventional single-cell analysis of cellular mechanical response was often conducted using two-dimensionally

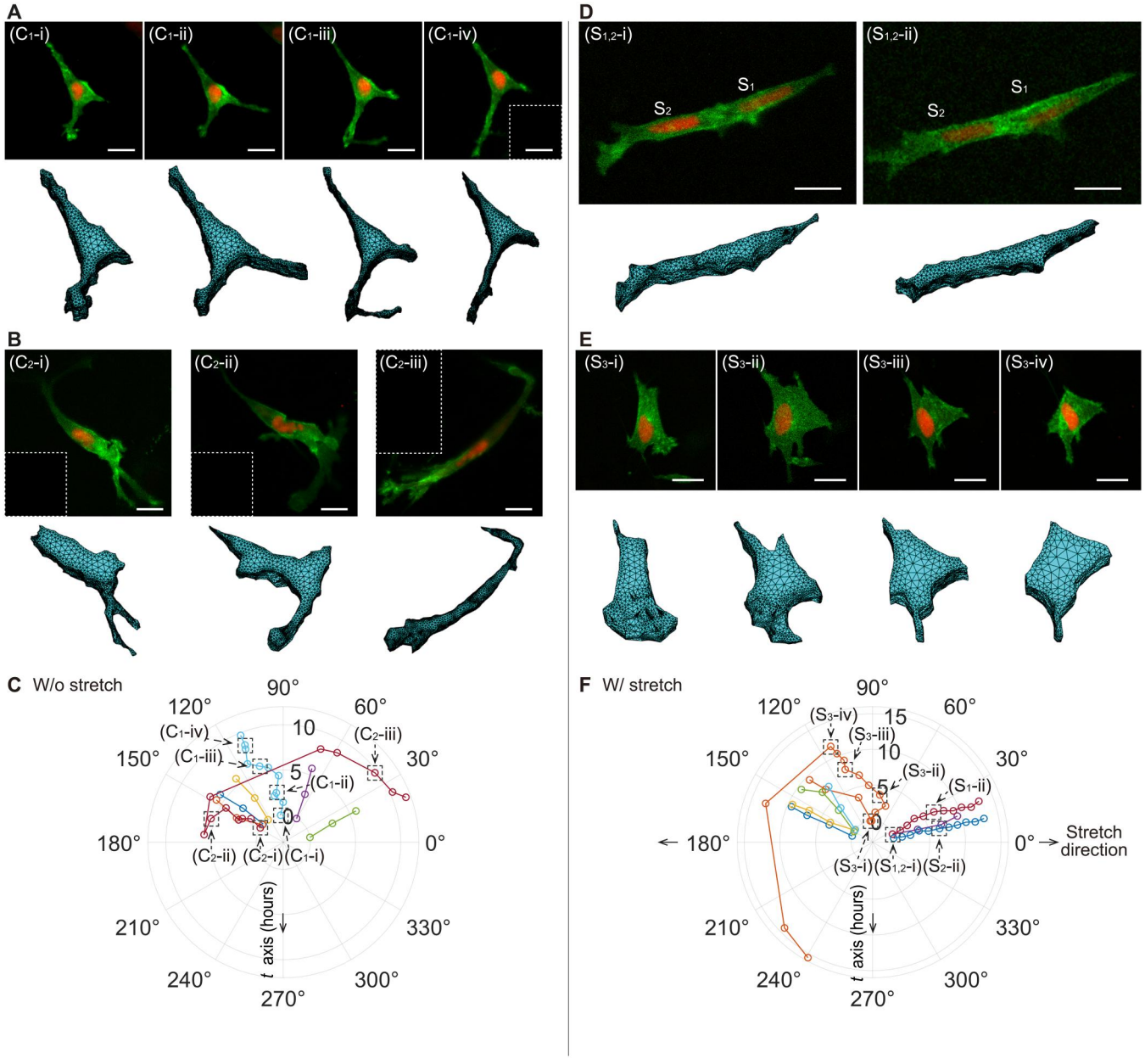

Fig. 6. Spatiotemporal single-cell tracking analysis in 3DMTs under mechanical stretch. (**A**) Acquired fluorescence images and reconstructed 3D models of cell C_1 at four different time points. The white dashed box indicates the area where an adjacent cell was cleared. (**B**) Acquired fluorescence images and reconstructed 3D models of cell C_2 at three different time points. The white dashed boxes indicate the area where adjacent cells were cleared. (**C**) Temporal change of nuclei angle of cells C_1 and C_2 and five other observed cells plotted in the polar plot. (**D**) Acquired fluorescence images and reconstructed 3D models of cells S_1 and S_2 at two different time points. (**E**) Acquired fluorescence images and reconstructed 3D models of cell S_3 at four different time points. (**F**) Temporal change of nuclei angle of cells S_1, S_2, and S_3 and six other observed cells plotted in the polar plot (all scale bars, 20 μm).

cultured cells and tissues due to the simpler experimental setups and the number of available equipment such as atomic force microscopy to measure cellular elasticity and calcium imaging to visualize intracellular mechanical response (*34*, *35*). 3D tissues, on the other hand, are troublesome to investigate because of several challenges; first, imaging of a single cell inside 3D tissues at a high resolution; and, second, focusing on the same target cell during exposure to mechanical stimuli, which was not resolved by previous research (*36*, *37*). Our system comprises the symmetrical stretch machine to keep focusing on a target cell under mechanical stretch and confocal microscopy to focus on a cell inside 3D tissues. The stretch machine composed of two linear motorized stages allows the application of mechanical stimuli with different patterns and frequencies, enabling the detailed investigation of stretch pattern–dependent cellular behavior and mechanical response. We also used C2C12 cells labeled with fluorescence to construct 3DMTs and successfully showed that it is possible to exclusively label a certain amount of cells in 3D tissues and

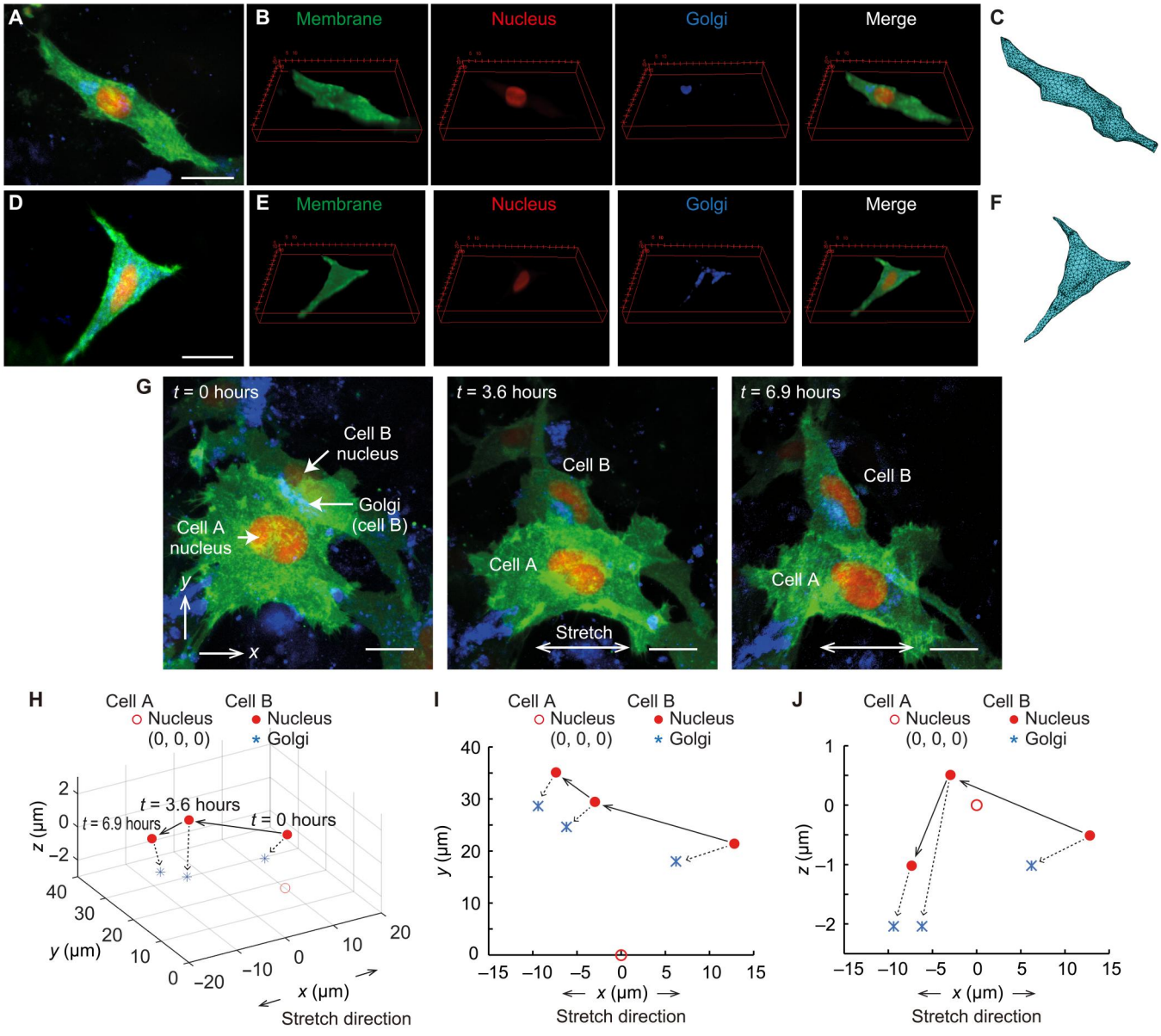

Fig. 7. Analysis of Golgi marker by spatiotemporal single-cell tracking. (**A**) The *z*-projected image of an observed cell with the localized Golgi at one side of the nucleus (membrane, green; nucleus, red; Golgi, blue). (**B**) 3D view of membrane, nucleus, and Golgi, and the merged view. (**C**) The 3D cell model reconstructed from the image stack of the membrane. (**D**) The *z*-projected image of an observed cell with the splitting Golgi around the nucleus. (**E**) 3D view of membrane, nucleus, and Golgi, and the merged view. (**F**) The 3D cell model reconstructed from the image stack of the membrane. (**G**) Two cells (cells A and B) were analyzed to see the relative position of cell B from cell A. Cell B had the fluorescently labeled Golgi. (**H** to **J**) The relative position of the nucleus and Golgi of cell B from the nucleus of cell A represented in the *xyz* plot, the *xy* plot, and the *xz* plot, respectively (all scale bars, 20 μm).

observe target cells at the single-cell level. The type of ECM is easily changeable to a variety of other gels, such as GelMA and fibril, enabling the investigation of cellular behavior in different ECMs. The *z*-stack images of target cells could be acquired and used for the reconstruction of the 3D cellular model to visualize cellular shape in 3D space (Fig. 6). Hopefully, further improvements could be done to the system; for example, the resolution of the acquired *z*-stack images is dependent on the resolution of confocal microscopy in the *z* direction (*38*), and the time required for *z*-stack acquisition limits the time resolution. By using confocal microscopy with a higher *z* resolution and a high-speed camera, it is expected to gain *z*-stack images with higher spatiotemporal resolution (*39*, *40*). The proposed analytical system is also limited by its low throughput due to our approach of fluorescently labeling a certain amount of cells in 3D tissues. While the transfection efficiency of 10 to 15% allows us to visually isolate a single cell and observe its entire structure without being overlapped by other surrounding cells, it also means that a limited number of cells can be observed per experiment, resulting in low throughput. However, this limitation can be overcome by incorporating laboratory automation, which is

becoming increasingly available, into our analysis system (*41*, *42*). By automating the analysis and observing more cells, we believe that the difference between without and with stretch will become more visible even in single-cell analysis and that the distribution will eventually converge to a histogram similar to the one obtained from the multicell-scale analysis (Fig. 4C).

The presented analysis for the investigation of cellular heterogeneity in 3D tissues has further potential to understand the mechanism of multiscale cellular response from a dynamic perspective. For instance, we assumed that different inputs of mechanical stimuli applied to each cell lead to heterogeneous cellular behavior. By fluorescently labeling ECM and imaging ECM dynamics simultaneously, it might be possible to measure the deformation of ECM and calculate the actual mechanical input applied to each cell (*43*). Together with the calculated mechanical input on cells and reconstructed 3D cellular models, the mechanical dynamics of every single cell could also be numerically calculated with computational simulation (*44*).

Moreover, our system and analysis have an immense impact on the research in mechanotransduction. When cells are exposed to mechanical stimuli, cells sense the stimuli via mechanoreceptors and mechanoresponsive signaling pathways are up-regulated/down-regulated, resulting in the activation/deactivation of certain molecules (*45*, *46*). The shift of molecule levels leads to changes in cellular behavior, such as migration and morphological changes. Spatiotemporally quantifying the level of these molecules is, therefore, crucial in understanding further details of mechanotransduction. For spatial quantification, spatial transcriptomics (ST) techniques attracted attention, due to the capability to spatially measure gene activity in a multicellular tissue sample (*47*). Even recently, a live cell tagging method for ST was developed, allowing the spatial gene activity mapping linked with the temporal cellular behavior (*48*). Together with our proposed analysis, it is anticipated to fully visualize the gene activity associated with local cellular/tissue behavior induced by mechanical stimuli. This could provide the whole information on mechanotransduction in multicellular systems that any other analytical methods have yet to offer.

To conclude, by expanding the scales from mechanical input at the single-cell level to the multicell tissue level, it is anticipated to understand the cell-tissue concerted mechanical response, leading to a comprehensive understanding of the mechanism behind mechanical stimuli–induced tissue structuring. With further improvements, we believe that the investigation of cellular heterogeneity will become a principal method to break through toward the development of tissue engineering.

MATERIALS AND METHODS

Fabrication of PDMS stretch chamber

PDMS stretch chamber was fabricated by simple PDMS molding and bonding of two layers: a top and a bottom layer. Molds for both layers were designed with 3D CAD software (SolidWorks, Dassault Systèmes, Vélizy-Villacoublay, France). An acrylic mold was prepared by machining and used for PDMS molding of the top layer (fig. S1A). For the bottom layer, an aluminum mold with tape spacers was prepared by machining (fig. S1D). Aluminum was used as the material for the bottom layer instead of acrylic as organic solvents might be used in the later procedure in PDMS peeling, and acrylic is prone to such solvents. The PDMS prepolymer was prepared by mixing the PDMS base liquid and curing agent (SYLGARD 184, Dow Corning, USA) in a ratio of 10:1 and then poured over the molds (fig. S1, B and E). To fabricate a thin bottom layer for optical observation at high resolution, the casted PDMS on the mold was compressed with a glass slide, resulting in the thickness of the bottom layer to thinner than 100 μm (fig. S1E). After heating at 75°C for 1.5 hours, the cured top and bottom layers were peeled off from the molds (fig. S1, C and F). The two layers were bonded with uncured PDMS and additional heating at 75°C for 1 hour to obtain the PDMS stretch chamber (fig. S1G). The chamber was washed with ethanol and then sterilized by autoclaving at 121°C for 20 min for further cell culture.

Cell preparation

The mouse myoblast C2C12 cell line (CRL-1772, American Type Culture Collection, Manassas, USA) was cultured in high-glucose Dulbecco's modified Eagle's medium (FUJIFILM WAKO Pure Chemical Corporation, Osaka, Japan) containing 10% fetal bovine serum (HyClone, Logan, USA) and 1% penicillin-streptomycin (Sigma-Aldrich, St. Louis, USA) in a humidified atmosphere incubator at 37°C with 5% CO_2. Cells were passaged before reaching 80% confluence to avoid cell differentiation. C2C12 cells were rinsed with phosphate-buffer saline (FUJIFILM WAKO Pure Chemical Corporation, Osaka, Japan) and treated with 0.25% trypsin-EDTA (Thermo Fisher Scientific, Waltham, USA) for detachment from dishes. The fresh medium was added, and the cell suspension was centrifuged at 130*g* for 5 min to collect cells. The cells were passaged several times before experiments to ensure stable proliferation.

For live cell imaging experiments, we introduced plasmid DNA (ßact2-nls-mCherry-IRES-EGFP-CAAX) into C2C12 cells to label cell membrane with EGFP [maximum excitation wavelength (λ_{Ex}) = 488 nm and maximum emission wavelength (λ_{Em}) = 509 nm] and nuclei with mCherry (λ_{Ex} = 587 nm and λ_{Em} = 610 nm). To transfect plasmid DNA into cells, a DNA complex was prepared by mixing 3 μl of TransIT-X2 Dynamic Delivery System reagent (MIR6003, Mirus, Madison, USA), 1 μg of the plasmid DNA, and 100 μl of Opti-MEM I Reduced Serum Medium (Thermo Fisher Scientific, Waltham, USA) and added to a ϕ35-mm cell culture dish filled with 1 ml of medium. After incubation for 3 to 4 hours, the cell medium was replaced with a fresh medium, followed by overnight incubation. For the transfection efficiency determination, cells were stained with 4′,6-diamidino-2-phenylindole (DAPI), and cell numbers were counted to derive the transfection efficiency by dividing the number of cells with mCherry-labeled nuclei by the number of cells with DAPI-stained nuclei. An additional plasmid DNA (pCMV6-AC-mBFP, OriGene Technologies Inc., Rockville, USA) labeling Golgi with BFP (λ_{Ex} = 374 nm and λ_{Em} = 443 nm) was used for live cell imaging with Golgi. Two DNA plasmids were added at 0.5 μg each to a DNA complex for cotransfection.

3D tissue culture in PDMS stretch chamber

A reconstitution buffer for collagen was prepared by mixing 50 mM sodium bicarbonate (Wako Pure Chemical Industries, Osaka, Japan), 260 mM sodium hydroxide bicarbonate (Wako Pure Chemical Industries, Osaka, Japan), and 200 mM Hepes (Dojindo, Kumamoto, Japan). The pre-gel collagen solution was prepared by mixing type I collagen (5 mg/ml; IAC-50, KOKEN, Tokyo, Japan), Hanks' balanced salt solution (Sigma-Aldrich, St. Louis, USA), and the reconstitution buffer in a volume ratio of 8:1:1, resulting in a solution

of 4 mg/ml. A mixture of the pre-gel collagen solution and Matrigel (10 mg/ml; Corning, New York, USA) was prepared in a volume ratio of 9:1 to prepare an ECM for constructing 3DMTs in the PDMS chamber (final concentration of 4.6 mg/ml). When preparing a sample with fluorescently stained collagen fibers in the ECM, the prepared pre-gel collagen solution was mixed with a fluorescent dye (Alexa Fluor 350 NHS, Thermo Fisher Scientific, Waltham, USA) in a volume ratio of 200:1 and incubated on ice for 1 hour, before mixing with Matrigel. After centrifuging the cell suspension and removing the medium, cells were suspended in the desired amount of the ECM to achieve a final cell concentration of 1.0×10^7 cells/ml. The cell-ECM mixture was loaded in the PDMS stretch chamber and allowed to polymerize for 15 min at 37°C. After polymerization, the medium was added to the chamber. The cells were cultured in a humidified atmosphere incubator at 37°C with 5% CO_2 for 1 day.

Stretch culture of 3D tissues and observation of cellular orientation

To conduct a stretch culture of 3DMTs, we used a lab-developed stretch machine composed of two linear motorized stages (TANN40-10C, SIGMAKOKI, Tokyo, Japan) operated from a controller (HSC-103, SIGMAKOKI, Tokyo, Japan) and PC (*25*). The PDMS stretch chamber was fixed on the stretch machine and subjected to uniaxial cyclic stretch (10%, 1 Hz) for 12 hours in a humidified environment at 37°C with 5% CO_2. Right before and after the stretch, cells were imaged with confocal microscopy (FV3000, OLYMPUS, Tokyo, Japan) and a 20× objective lens (UPLSAPO 20X, OLYMPUS, Tokyo, Japan) to acquire multicell-scale *z*-stack images to evaluate cellular orientation.

Spatiotemporal live imaging of 3D tissues at a single-cell scale under mechanical stretch

The developed optical live imaging system of single cells in the 3D tissue under mechanical stretch was composed of confocal microscopy, a custom-made stage-top incubator, and two linear motorized stages (fig. S5A). The stage-top incubator was established by integrating an incubation system (INUBG2-ONICSH2, Tokai Hit, Shizuoka, Japan) with a surrounding acrylic incubator and an additional heater on top (fig. S5B). The temperatures of the heaters were adjusted so that the temperature of the medium in the PDMS stretch chamber reached 37°C. During the experiment, the medium heated to 37°C was added every 2 hours to compensate for the evaporation of the medium. Objective lenses (40×; UPLSAPO 40X2 dry lens or UAPON 40XW340 water immersion lens, OLYMPUS, Tokyo, Japan) were used for the observation and acquisition of the *z*-stack images.

Image analysis

All the acquired confocal fluorescence images were processed and analyzed with Fiji (*49*), a distribution of ImageJ (National Institutes of Health, Maryland, USA). *Z*-stack images of nuclei were converted to 8-bit grayscale and projected in a single image. The nuclei in the projected images were binarized with thresholding, denoised with a median filter, and fitted to ellipses. The nuclei angle was determined by measuring the angle between the major axis of the fitted ellipse and the stretch direction. The center coordinates of the fitted ellipses were measured as the position of nuclei and used to determine the distance between two cells. *Z*-stack images of the membrane were converted to 8-bit grayscale, projected in a single image, binarized, denoised with a median filter, and fitted to an ellipse to measure the angle between the major axis and the stretch direction, the length of the major and minor axes. *Z*-stack images of Golgi were converted to 8-bit grayscale, projected in a single image, binarized, and denoised with a median filter to determine a centroid position. The *z* position of nuclei and Golgi were determined by choosing an image slice with the highest intensity in a *z* stack. The orientation of collagen fibers was characterized by processing confocal images of collagen with OrientationJ ImageJ plugins (*50*, *51*). The images of collagen were denoised with Lpx filter 2d in LPIXEL ImageJ plugins (LPIXEL Inc., Tokyo, Japan) before the measurement of orientation (*52*). Acquired image stacks of cells were visualized with 3D viewer plugin (*53*).

Reconstruction of 3D cellular models from acquired image stacks

3D cellular models were reconstructed from acquired *z*-stack images of the cellular membrane by using MATLAB (MathWorks, Massachusetts, USA). As a preparation for the 3D model reconstruction, the cells to be analyzed were cropped from *z*-stack images, and surrounding cells were cleared. A median filter was applied to reduce noise, and brightness and contrast were adjusted manually. In the case of confocal images obtained with the 40× dry lens, the intensity of all slices in the *z* stack was measured for each cell to choose an image slice with the highest intensity as a middle slice (fig. S6). Then, five slice images each above and below the middle slice image, in total 11 slice images, were used for the image projection in a single image and the reconstruction of a 3D cellular model (fig. S6). In the case of the 40× water immersion lens, a total of 31 slice images were used for the 3D model reconstruction because of a higher *z* resolution. The selected slices were loaded on MATLAB to find boundary points describing the contours of cells and create a 3D volume using the alphaShape function. To acquire a 3D cellular model with triangular meshes, a matrix representing the boundary of the alpha shape was acquired using the boundaryFacets function, and an STL file was created and visualized using the stlwrite function and Partial Differential Equation Toolbox (MathWorks, Massachusetts, USA).

Statistical analysis

The K-S tests were used for data comparison. The calculated *P* value was stated in the figure. n.s. denotes not significant.

Supplementary Materials

This PDF file includes:

Figs. S1 to S6
Supplementary Materials and Methods
References

REFERENCES AND NOTES

1. A. M. Cheung, L. Giangregorio, Mechanical stimuli and bone health: What is the evidence? *Curr. Opin. Rheumatol.* **24**, 561–566 (2012).
2. K. M. Wisdom, S. L. Delp, E. Kuhl, Use it or lose it: Multiscale skeletal muscle adaptation to mechanical stimuli. *Biomech. Model. Mechanobiol.* **14**, 195–215 (2015).
3. P. A. Janmey, C. A. McCulloch, Cell Mechanics: Integrating cell responses to mechanical stimuli. *Annu. Rev. Biomed. Eng.* **9**, 1–34 (2007).

4. C. Souilhol, J. Serbanovic-Canic, M. Fragiadaki, T. J. Chico, V. Ridger, H. Roddie, P. C. Evans, Endothelial responses to shear stress in atherosclerosis: A novel role for developmental genes. *Nat. Rev. Cardiol.* **17**, 52–63 (2020).
5. Y. Ma, S. Fu, L. Lu, X. Wang, Role of androgen receptor on cyclic mechanical stretch-regulated proliferation of C2C12 myoblasts and its upstream signals: IGF-1-mediated PI3K/Akt and MAPKs pathways. *Mol. Cell. Endocrinol.* **450**, 83–93 (2017).
6. Y.-J. Chang, Y.-J. Chen, C.-W. Huang, S.-C. Fan, B.-M. Huang, W.-T. Chang, Y.-S. Tsai, F.-C. Su, C.-C. Wu, Cyclic stretch facilitates myogenesis in C2C12 myoblasts and rescues thiazolidinedione-inhibited myotube formation. *Front. Bioeng. Biotechnol.* **4**, 27 (2016).
7. F. Wang, Z.-L. Wei, X.-R. Sun, Q. Zhang, C.-X. Zhang, W.-X. Jiang, X. Yan, J.-N. Liu, X. Yuan, Apoptosis inducing factor is involved in stretch-induced apoptosis of myoblast via a caspase-9 independent pathway. *J. Cell. Biochem.* **118**, 829–838 (2017).
8. C. Rinoldi, M. Costantini, E. Kijeńska-Gawrońska, S. Testa, E. Fornetti, M. Heljak, M. Ćwiklińska, R. Buda, J. Baldi, S. Cannata, J. Guzowski, C. Gargioli, A. Khademhosseini, W. Swieszkowski, Tendon tissue engineering: Effects of mechanical and biochemical stimulation on stem cell alignment on cell-laden hydrogel yarns. *Adv. Healthc. Mater.* **8**, e1801218 (2019).
9. M. Furuhashi, Y. Morimoto, A. Shima, F. Nakamura, H. Ishikawa, S. Takeuchi, Formation of contractile 3D bovine muscle tissue for construction of millimetre-thick cultured steak. *NPJ Sci. Food* **5**, 6 (2021).
10. S. Asano, S. Ito, M. Morosawa, K. Furuya, K. Naruse, M. Sokabe, E. Yamaguchi, Y. Hasegawa, Cyclic stretch enhances reorientation and differentiation of 3-D culture model of human airway smooth muscle. *Biochem. Biophys. Rep.* **16**, 32–38 (2018).
11. K. H. Nakayama, M. Shayan, N. F. Huang, Engineering biomimetic materials for skeletal muscle repair and regeneration. *Adv. Healthc. Mater.* **8**, e1801168 (2019).
12. C. Rinoldi, A. Fallahi, I. K. Yazdi, J. Campos Paras, E. Kijeńska-Gawrońska, G. Trujillo-de Santiago, A. Tuoheti, D. Demarchi, N. Annabi, A. Khademhosseini, W. Swieszkowski, A. Tamayol, Mechanical and biochemical stimulation of 3D multilayered scaffolds for tendon tissue engineering. *ACS Biomater Sci. Eng.* **5**, 2953–2964 (2019).
13. W. Zhang, C. W. Kong, M. H. Tong, W. H. Chooi, N. Huang, R. A. Li, B. P. Chan, Maturation of human embryonic stem cell-derived cardiomyocytes (hESC-CMs) in 3D collagen matrix: Effects of niche cell supplementation and mechanical stimulation. *Acta Biomater.* **49**, 204–217 (2017).
14. N. Bono, D. Pezzoli, L. Levesque, C. Loy, G. Candiani, G. B. Fiore, D. Mantovani, Unraveling the role of mechanical stimulation on smooth muscle cells: A comparative study between 2D and 3D models. *Biotechnol. Bioeng.* **113**, 2254–2263 (2016).
15. K. Y. Morgan, L. D. Black 3rd, Investigation into the effects of varying frequency of mechanical stimulation in a cycle-by-cycle manner on engineered cardiac construct function. *J. Tissue Eng. Regen. Med.* **11**, 342–353 (2017).
16. C. Mueller, M. Trujillo-Miranda, M. Maier, D. E. Heath, A. J. O'Connor, S. Salehi, Effects of external stimulators on engineered skeletal muscle tissue maturation. *Adv. Mater. Interfaces* **8**, 2001167 (2021).
17. Z. E. Goldblatt, H. Ashouri Choshali, H. A. Cirka, V. Liang, Q. Wen, D. McCollum, N. Rahbar, K. L. Billiar, Heterogeneity profoundly alters emergent stress fields in constrained multicellular systems. *Biophys. J.* **118**, 15–25 (2020).
18. M. Vishwakarma, B. Thurakkal, J. P. Spatz, T. Das, Dynamic heterogeneity influences the leader–follower dynamics during epithelial wound closure. *Philos. Trans. R. Soc. Lond. B Biol. Sci.* **375**, 20190391 (2020).
19. M. Jebeli, S. K. Lopez, Z. E. Goldblatt, D. McCollum, S. Mana-Capelli, Q. Wen, K. Billiar, Multicellular aligned bands disrupt global collective cell behavior. *Acta Biomater.* **163**, 117–130 (2023).
20. B. L. Khoo, P. K. Chaudhuri, N. Ramalingam, D. S. W. Tan, C. T. Lim, M. E. Warkiani, Single-cell profiling approaches to probing tumor heterogeneity. *Int. J. Cancer* **139**, 243–255 (2016).
21. H. Zheng, Y. Pomyen, M. O. Hernandez, C. Li, F. Livak, W. Tang, H. Dang, T. F. Greten, J. L. Davis, Y. Zhao, M. Mehta, Y. Levin, J. Shetty, B. Tran, A. Budhu, X. W. Wang, Single-cell analysis reveals cancer stem cell heterogeneity in hepatocellular carcinoma. *Hepatology* **68**, 127–140 (2018).
22. Y. Kim, H. Ko, I. K. Kwon, K. Shin, Extracellular matrix revisited: Roles in tissue engineering. *Int. Neurourol. J.* **20**, S23–S29 (2016).
23. A. Khodabukus, N. Prabhu, J. Wang, N. Bursac, In vitro tissue-engineered skeletal muscle models for studying muscle physiology and disease. *Adv. Healthc. Mater.* **7**, e1701498 (2018).
24. J. W. Fleming, A. J. Capel, R. P. Rimington, D. J. Player, A. Stolzing, M. P. Lewis, Functional regeneration of tissue engineered skeletal muscle in vitro is dependent on the inclusion of basement membrane proteins. *Cytoskeleton* **76**, 371–382 (2019).
25. A. Shimizu, W. H. Goh, S. Itai, M. Hashimoto, S. Miura, H. Onoe, ECM-based microchannel for culturing in vitro vascular tissues with simultaneous perfusion and stretch. *Lab Chip* **20**, 1917–1927 (2020).
26. D. J. Player, N. R. W. Martin, S. L. Passey, A. P. Sharples, V. Mudera, M. P. Lewis, Acute mechanical overload increases IGF-I and MMP-9 mRNA in 3D tissue-engineered skeletal muscle. *Biotechnol. Lett.* **36**, 1113–1124 (2014).
27. K. Chen, A. Vigliotti, M. Bacca, R. M. McMeeking, V. S. Deshpande, J. W. Holmes, Role of boundary conditions in determining cell alignment in response to stretch. *Proc. Natl. Acad. Sci. U.S.A.* **115**, 986–991 (2018).
28. C. He, M. Liu, D. Jiang, J. Wu, C. Qin, T. Liang, P. Wu, C. Han, L. Huang, K. J. Hsia, P. Wang, Fabricating tissues in situ with the controlled cellular alignments. *Adv. Healthc. Mater.* **11**, e2100934 (2022).
29. A. Tondon, R. Kaunas, The direction of stretch-induced cell and stress fiber orientation depends on collagen matrix stress. *PLOS ONE* **9**, e89592 (2014).
30. A. Livne, E. Bouchbinder, B. Geiger, Cell reorientation under cyclic stretching. *Nat. Commun.* **5**, 3938 (2014).
31. T. Mao, Y. He, Y. Gu, Y. Yang, Y. Yu, X. Wang, J. Ding, Critical frequency and critical stretching rate for reorientation of cells on a cyclically stretched polymer in a microfluidic chip. *ACS Appl. Mater. Interfaces* **13**, 13934–13948 (2021).
32. S. Dhein, A. Schreiber, S. Steinbach, D. Apel, A. Salameh, F. Schlegel, M. Kostelka, P. M. Dohmen, F. W. Mohr, Mechanical control of cell biology. Effects of cyclic mechanical stretch on cardiomyocyte cellular organization. *Prog. Biophys. Mol. Biol.* **115**, 93–102 (2014).
33. T. Aoki, M. Nishita, J. Sonoda, T. Ikeda, Y. Kakeji, Y. Minami, Intraflagellar transport 20 promotes collective cancer cell invasion by regulating polarized organization of Golgi-associated microtubules. *Cancer Sci.* **110**, 1306–1316 (2019).
34. X. Shao, Q. Li, A. Mogilner, A. D. Bershadsky, G. V. Shivashankar, Mechanical stimulation induces formin-dependent assembly of a perinuclear actin rim. *Proc. Natl. Acad. Sci. U.S.A.* **112**, E2595–E2601 (2015).
35. J. Y. Shiu, L. Aires, Z. Lin, V. Vogel, Nanopillar force measurements reveal actin-cap-mediated YAP mechanotransduction. *Nat. Cell Biol.* **20**, 262–271 (2018).
36. Y. Li, G. Huang, M. Li, L. Wang, E. L. Elson, T. J. Lu, G. M. Genin, F. Xu, An approach to quantifying 3D responses of cells to extreme strain. *Sci. Rep.* **6**, 19550 (2016).
37. M. Walker, P. Rizzuto, M. Godin, A. E. Pelling, Structural and mechanical remodeling of the cytoskeleton maintains tensional homeostasis in 3D microtissues under acute dynamic stretch. *Sci. Rep.* **10**, 7696 (2020).
38. L. E. Smith, R. Smallwood, S. Macneil, A comparison of imaging methodologies for 3D tissue engineering. *Microsc. Res. Tech.* **73**, 1123–1133 (2010).
39. B. B. Straub, D. C. Lah, H. Schmidt, M. Roth, L. Gilson, H.-J. Butt, G. K. Auernhammer, Versatile high-speed confocal microscopy using a single laser beam. *Rev. Sci. Instrum.* **91**, 033706 (2020).
40. Z. Zhang, L. Bai, L. Cong, P. Yu, T. Zhang, W. Shi, F. Li, J. Du, K. Wang, Imaging volumetric dynamics at high speed in mouse and zebrafish brain with confocal light field microscopy. *Nat. Biotechnol.* **39**, 74–83 (2020).
41. B. Burger, P. M. Maffettone, V. V. Gusev, C. M. Aitchison, Y. Bai, X. Wang, X. Li, B. M. Alston, B. Li, R. Clowes, N. Rankin, B. Harris, R. S. Sprick, A. I. Cooper, A mobile robotic chemist. *Nature* **583**, 237–241 (2020).
42. G. N. Kanda, T. Tsuzuki, M. Terada, N. Sakai, N. Motozawa, T. Masuda, M. Nishida, C. T. Watanabe, T. Higashi, S. A. Horiguchi, T. Kudo, M. Kamei, G. A. Sunagawa, K. Matsukuma, T. Sakurada, Y. Ozawa, M. Takahashi, K. Takahashi, T. Natsume, Robotic search for optimal cell culture in regenerative medicine. *eLife* **11**, e77007 (2022).
43. A. D. Doyle, D. J. Sykora, G. G. Pacheco, M. L. Kutys, K. M. Yamada, 3D mesenchymal cell migration is driven by anterior cellular contraction that generates an extracellular matrix prestrain. *Dev. Cell* **56**, 826–841.e4 (2021).
44. Y. Yu, G. Bourantas, B. Zwick, G. Joldes, T. Kapur, S. Frisken, R. Kikinis, A. Nabavi, A. Golby, A. Wittek, K. Miller, Computer simulation of tumour resection-induced brain deformation by a meshless approach. *Int. J. Numer. Method. Biomed. Eng.* **38**, e3539 (2022).
45. K. Ohashi, S. Fujiwara, K. Mizuno, Roles of the cytoskeleton, cell adhesion and rho signalling in mechanosensing and mechanotransduction. *J. Biochem.* **161**, 245–254 (2017).
46. X. Liu, X. Liu, M. Li, Y. Zhang, W. Chen, M. Zhang, C. Zhang, M. Zhang, Mechanical stretch induces smooth muscle cell dysfunction by regulating ACE2 via P38/ATF3 and post-transcriptional regulation by miR-421. *Front. Physiol.* **11**, 540591 (2021).
47. B. L. Walker, Z. Cang, H. Ren, E. Bourgain-Chang, Q. Nie, Deciphering tissue structure and function using spatial transcriptomics. *Commun. Biol.* **5**, 220 (2022).
48. A. S. Genshaft, C. G. K. Ziegler, C. N. Tzouanas, B. E. Mead, A. M. Jaeger, A. W. Navia, R. P. King, M. D. Mana, S. Huang, V. Mitsialis, S. B. Snapper, Ö. H. Yilmaz, T. Jacks, J. F. Van Humbeck, A. K. Shalek, Live cell tagging tracking and isolation for spatial transcriptomics using photoactivatable cell dyes. *Nat. Commun.* **12**, 4995 (2021).
49. J. Schindelin, I. Arganda-Carreras, E. Frise, V. Kaynig, M. Longair, T. Pietzsch, S. Preibisch, C. Rueden, S. Saalfeld, B. Schmid, J. Y. Tinevez, D. J. White, V. Hartenstein, K. Eliceiri, P. Tomancak, A. Cardona, Fiji: An open-source platform for biological-image analysis. *Nat. Methods* **9**, 676–682 (2012).

50. Z. Püspöki, M. Storath, D. Sage, M. Unser, Transforms and operators for directional bioimage analysis: A survey. *Adv. Anat. Embryol. Cell Biol.* **219**, 69–93 (2016).
51. R. Rezakhaniha, A. Agianniotis, J. T. C. Schrauwen, A. Griffa, D. Sage, C. V. C. Bouten, F. N. van de Vosse, M. Unser, N. Stergiopulos, Experimental investigation of collagen waviness and orientation in the arterial adventitia using confocal laser scanning microscopy. *Biomech. Model. Mechanobiol.* **11**, 461–473 (2012).
52. H. Ueda, E. Yokota, N. Kutsuna, T. Shimada, K. Tamura, T. Shimmen, S. Hasezawa, V. V. Dolja, I. Hara-Nishimuraa, Myosin-dependent endoplasmic reticulum motility and F-actin organization in plant cells. *Proc. Natl. Acad. Sci. U.S.A.* **107**, 6894–6899 (2010).
53. B. Schmid, J. Schindelin, A. Cardona, M. Longair, M. Heisenberg, A high-level 3D visualization API for Java and ImageJ. *BMC Bioinformatics* **11**, 274 (2010).
54. C. B. Raub, A. J. Putnam, B. J. Tromberg, S. C. George, Predicting bulk mechanical properties of cellularized collagen gels using multiphoton microscopy. *Acta Biomater.* **6**, 4657–4665 (2010).

Acknowledgments
Funding: This work was partly supported by Grant-in-aid for Scientific Research (A)(19H01178) and (A)(23H00555), Japan Society for the Promotion of Science (JSPS), and Takahashi Industrial and Economic Research Foundation. **Author contributions:** K.K., Y.K., and H.O. conceived the project, designed the study, and interpreted the results. K.K. performed all the experiments and data analyses. J.M. conducted the analysis on the mechanical property of ECM and performed the tissue culture experiment with K.K. S.Miu. contributed to the transfection using plasmid DNA. S.Mi. contributed to the design of the optical live imaging and stretch system. K.K., Y.K., and H.O. wrote the paper. All authors discussed the results and commented on the manuscript. **Competing interests:** The authors declare that they have no competing interests. **Data and materials availability:** All data needed to evaluate the conclusions in the paper are present in the paper and/or the Supplementary Materials.

Submitted 25 November 2022
Accepted 8 September 2023
Published 13 October 2023
10.1126/sciadv.adf9917